JOURNAL OF AIRCRAFT
Vol. 36, No. 6, November–December 1999

Experimental Heat Transfer Coefficients from Ice-Roughened Surfaces for Aircraft Deicing Design

Nihad Dukhan,* K. C. Masiulaniec,† and Kenneth J. De Witt‡
University of Toledo, Toledo, Ohio 43606
and
G. James Van Fossen Jr.§
John H. Glenn Research Center at Lewis Field, Cleveland, Ohio 44135

Experimental Stanton numbers are presented for seven aluminum model castings of ice-roughened surfaces in parallel air flow for Re_x ranging from 5.3×10^4 to 1.3×10^6. The Stanton numbers were generally higher than those for previous studies with hemispherical and truncated cone roughness elements, and the majority of the data were in the fully turbulent regime. In general, the rime feather ice roughness produced the highest rate of heat transfer, followed by the rough glaze roughness, the smooth rime roughness, and the smooth glaze roughness, respectively. In the fully developed turbulent regime the local Stanton number could be described by a power law of the form $St_x = a\,Re_x^m\,Pr^{-0.4}$ where a and m correlated well with the newly defined Index of Random Roughness and the roughness height, respectively. This work provides a set of measured values of the Stanton number, specific to the case of stochastically accreted ice on aircraft surfaces, needed for the effective design of in-flight deicing systems.

Nomenclature

A = surface area
a = constant for correlations in Eqs. (4) and (5)
c_p = specific heat of air at constant pressure
d = diameter of hemispheres of Hosni et al.[6,8]
$\bar{H}$ = average roughness element height for a roughness model
h = heat-transfer coefficient
k = thermal conductivity of air
L = roughness elements spacing in Hosni et al.[6,8]
m = constant for correlations in Eqs. (4) and (6)
n = constant for correlations in Eq. (4)
Pr = Prandtl number, $c_p\mu/k$
Re_x = local Reynolds number, $u_\infty x/\nu$
$\bar{S}$ = average spacing of roughness elements for a roughness model
St_x = local Stanton number, $h/\rho c_p u_\infty$
T = temperature
u = mean axial velocity
x = axial distance from the leading edge along the surface
η = constant for correlations in Eq. (4)
μ = dynamic viscosity of air
ν = kinematic viscosity of air
ρ = density of air
ϕ = constant for correlations in Eq. (4)

Subscripts

o = unheated
rgh = rough
s = surface
smth = smooth
t = tunnel
x = axial, horizontal, streamwise direction
∞ = freestream

Introduction

THE fluid dynamics and the thermal behavior of any internal or external flow are extremely sensitive to the roughness condition of the solid surface. The fluid drag and the heat transfer are usually higher when the surface is rough. One of the many practical applications, and the objective of this study, is the roughness problem associated with ice accretion on aircraft surfaces.

The effect of surface roughness on fluid flow and heat transfer has been a subject of historical interest. To artificially roughen their test surfaces, researchers used easily available and measurable objects. Nikuradse,[1] for example, launched the first experimental study to determine the frictional effect of sand grain roughness on water flow in pipes of different diameters. Schlichting[2] investigated the roughness caused by spheres, cones, and transverse steel angles. The frictional resistance depended upon the height and the roughness density, which was the number of roughness elements per unit area. The equivalent sand grain roughness was also defined by Schlichting as the grain size of the sand roughness as used in the test of Nikuradse that had the same resistance to the flow as the corresponding roughness elements at the same gross Reynolds number based on the hydraulic radius.

In subsequent investigations authors used Nikuradse's and Schlichting's results and the equivalent sand grain roughness concept to analyze their experimental data and to develop their empirical models, e.g., Simpson.[3] Numerical solutions were also developed by utilizing the equivalent sand grain approach (see Ref. 4). Coleman et al.,[5] however, showed that Schlichting had made erroneous assumptions in his data reduction. The values of the equivalent sand grain roughness used by Schlichting were too high by amounts ranging from 26 to 555%. Hosni et al.[6] utilized a new predictive numerical approach called the discrete element method to overcome difficulties associated with the equivalent sand grain approach. Lewis[7] provided an analytical treatment of the turbulent shear flow over a well-defined rough surface composed of evenly spaced rectangular ribs. In this analytical model the flowfield was treated as a series of attached and separated flow regions. The momentum and heat-transfer characteristics for the rough surface were presented.

Presented as Paper 96-0867 at the AIAA 34th Aerospace Sciences Meeting, Reno, NV, 15–19 January 1996; received 7 April 1998; revision received 25 November 1998; accepted for publication 21 February 1999.

*Graduate Student; currently, Senior Engineer at RELTEC Corporation, 4350 Weaver Parkway, Warrenville, IL 60555-3930.
†Associate Professor, Department of Mechanical, Industrial and Manufacturing Engineering. Member AIAA.
‡Professor, Department of Chemical Engineering.
§Senior Research Scientist. Member AIAA.

Hosni et al.[6] presented heat-transfer data for turbulent boundary layer airflow over three rough surfaces composed of 1.27×10^{-3} m diam hemispheres spaced 2, 4, and 10 diameters apart in staggered arrays for a local Reynolds number up to 10^7. Heat-transfer rates increased with increasing roughness density. The Stanton numbers for a given surface, at different freestream velocities, collapsed together when plotted against the local Reynolds number as the freestream velocity increased.

Hosni et al.[8] reported experimental Stanton number and skin-friction coefficient results for zero pressure gradient incompressible turbulent boundary-layer airflows over two rough surfaces composed of 1.27×10^{-3} m base diameter $\times 6.35 \times 10^{-4}$ m high truncated cones. The cones were spaced in staggered arrays two and four base diameters apart for freestream velocities ranging from 6 to 66 m/s. In general, the Stanton numbers for the conical roughness were about 4% lower than those for the hemisphere roughness obtained by Hosni et al.[6]

Coleman[9] investigated the behavior of the fully rough turbulent boundary layer subject to favorable pressure gradients over a porous test surface composed of densely packed spheres of uniform size (1.27×10^{-3} m diam). Profiles of mean velocity, mean temperature, and the components of the Reynolds stress tensor were reported. A new acceleration parameter was defined and was shown to be dependent on the roughness size but independent of molecular viscosity. For high enough Reynolds numbers acceleration caused an increase in the Stanton number. The possibility of having an equilibrium thermal state for the case of constant-wall temperature was stressed. This state was characterized by similar temperature profiles in the flow direction and a constant Stanton number.

In a different study Hosni et al.[10] gave predictions and measurements of the effect of surface roughness on the turbulent rough-wall boundary layer. The cases considered were constant-wall temperature, constant-wall heat flux, step-wall temperature, and piecewise linear-wall temperature distributions. Some accelerated flow cases were also investigated. A modified roughness energy transport model for the discrete element prediction method was presented.

Poinsatte[11,12] presented experimental heat-transfer data from both smooth and roughened NACA 0012 airfoils for chord Reynolds numbers in the range 1.24×10^6–2.50×10^6 and various angles of attack up to 4 deg. Roughness was obtained by attaching 2-mm-diam hemispheres arranged in four different patterns. The roughness, in general, drastically increased the heat-transfer rates. Moreover, increasing the density of the roughness elements from the sparse to the dense pattern caused yet a higher increase in heat transfer ranging from 32 to 54%. Increasing the angle of attack also caused heat transfer to increase over the 0-deg case, and the angle of attack dependence was much more prominent in the dense roughness case.

Pais et al.[13] used wind-tunnel measurements to obtain the local convective heat-transfer coefficients for 0- (smooth) and 5-min glaze-like ice models on a NACA 0012 airfoil. The chord Reynolds number range was from 7×10^5 to 2×10^6. Their results for the 5-min model showed that the maximum Nusselt number occurred at the tip of the glaze horn, where it was 51% higher than the rest of the surface and 25% higher for the same location at time equals zero. No attempt was made to model the surface roughness of the glaze ice used to construct the model.

The severe degradations in aerodynamic performance associated with accreted ice on airfoil surfaces are well known. To utilize deicing or anti-icing systems, computational schemes that predict ice accretions rely on empirical relationships for the convective heat-transfer rates from the surface of the accreted ice with some corrections to account for the effect of roughness. Predictions of the ice growth rates and the resulting shapes, using these codes, are extremely sensitive to the values used for the heat-transfer coefficient. Ice accretion predictions by NASA's LEWICE, for example, call for refinement or replacement of the current empirical relationships (especially for glaze ice) with new relationships that give more representative or physically correct values of the convective heat-transfer coefficient.[14] This was the motivating problem for the current study to determine the heat-transfer characteristics of ice-roughened surfaces. This study produced direct, accurate, and well-posed experimental data sets of the convective heat-transfer coefficient from roughened surfaces, which are important for their intrinsic value and are also essential, as just mentioned, for numerical codes that simulate ice accretion. Additionally, however, a knowledge of the range of heat losses that may be expected with different types of ice accretions provides the information required to effectively size and design different types of in-flight deicing systems. For electrothermal deicing systems this provides the information needed to specify heater mat densities and firing strategies.

Experiment

Investment Casting

Different ice accretions were obtained on 0.458×0.458 m (18×18 in.) flat aluminum plates in the Icing Research Tunnel (IRT) at the John H. Glenn Research Center at Lewis Field. Table 1 lists the icing tunnel conditions and the characterization of the resulting ice shapes for the four plates that provided the types of ice accretions which were used to construct the seven roughness models of this study, as listed in Table 2. Most of the plates had sectors of different types of ice accretions depending on the proximity to the leading edge.

Aluminum castings of these ice accretions were then meticulously obtained, with all of the microscopic details intact, using a modified

Table 1 Tunnel icing conditions and resulting ice characterization

Plate no.	T_t, °C	u_∞, m/s	LWC,[a] g/m^3	MVD,[b] μm	Spray time, min	Qualitative characterization of ice shapes	Center test tiles for roughness model no.
1	−1.11	67.05	1.0	30	2.0	Smooth glaze	6
2	−9.44	67.05	1.0	20	2.0	Smooth rime ice	5, 7
3	−1.11	67.05	1.3	30	6.0	Rough glaze	1, 2, 3
4	−9.44	67.05	1.0	20	8.0	Rime ice feather	4

[a]LWC (liquid water content in the icing wind tunnel). [b]MVD (median volume of drop size in the icing wind tunnel).

Table 2 Characterization of roughness

Model no.	Qualitative characterization of ice shapes	Average height, $\bar{H} \times 10^3$, m	Average spacing, $\bar{S} \times 10^3$, m	Area increase, A_{rgh}/A_{smth}	IRR	St_x increase over smooth model for $u_\infty = 47.2$ m/s, %
1	Closely-spaced rough glaze	1.88	2.39	1.44	1.13	601
2	Loosely-spaced rough glaze	2.87	15.09	1.18	0.22	621
3	Intermediately spaced rough glaze	3.07	5.56	1.43	0.79	602
4	Rime feathers	4.32	7.92	1.29	0.70	644
5	Closely spaced smooth rime	0.48	0.41	1.13	1.34	419
6	Smooth glaze	0.41	7.14	1.06	0.06	363
7	Smooth rime	1.09	3.96	1.08	0.30	451

investment casting technique. The investment casting process was used because it is most flexible with respect to attainable intricacy and precision (average tolerance $\pm 9.0 \times 10^{-5}$ m) (Ref. 15).

Each plate, with its accreted ice, was placed in a wooden box 0.458 m long × 0.458 m wide and 0.102 m deep. A special refractory mixture consisting of a substrate, a binder, and a gelling agent was then prepared. The substrate was a ceramic powder commercially known as R&R REFRACTOMIX NO. 1. This powder was specifically designed for use when fine detail transfer from the investment to the cast is critical, and hence it is largely used in the cast-to-size-tooling field. The binder was prehydrolyzed ethyl silicate commercially known as SILBOND H-5 and contained ethyl alcohol and methyl alcohol. The gelling agent was a 7.5% solution of ammonium carbonate in ammonium hydroxide. To avoid freezing at low temperatures, ethyl alcohol was chosen to suspend the mixture. The quantities of each ingredient necessary to avoid excessive shrinkage, warping, or inferior strength of the mold, and also to allow enough working time before solidification were weighed or measured carefully before mixing. The refractory mixture was then blended thoroughly with the proper proportions of the different ingredients while stirring as recommended by the manufacturer. The individual components and the final mixture were at a temperature lower than that of the accreted ice to avoid any melting of the ice. After thorough mixing the slurry was carefully and slowly poured over the ice shapes inside the wooden boxes without destroying the ice shapes' characteristics. Enough runny slurry was poured onto each plate until its thickness was about 0.038 m. The wooden boxes served the purpose of holding the slurry in place as solidification took place. The boxes were left in the tunnel for a few hours, then quickly moved to a freezer and left for 24 h to ensure complete curing of the mold. The dewaxing of these molds was rather simple. After complete cure the ice shapes were allowed to melt by moving the boxes outside the freezer and letting the ice shapes warm slowly to room temperature. Liquid water was poured out, and the molds were left for a few days to ensure complete solidification and drying. The molds were then ready for the investment casting phase.

Each refractory mold was placed in a furnace and was fired at a temperature of 649–760°C (1200–1400°F) for at least 2 h. Firing the mold served two purposes: it burned off any carbonaceous material present from the binder, and it preheated the mold for casting. After firing, each mold was allowed to cool to the desired casting temperature of approximately 427°C (800°F). Molten 356-aluminum at a higher temperature was then poured into each of the ceramic molds. The elevated temperature of the molds themselves ensured that the aluminum remained molten for a period of time so as to flow into the smaller cavities and capture as much of the microscopic surface detail as possible.

After complete solidification of the aluminum, the ceramic molds were broken off and separated from the aluminum plates. A high-pressure water jet was then used to remove all remaining traces of the ceramic material from the mold, especially in the small cavities.

Model Construction

To verify the classical heat-transfer coefficient values for a smooth, flat plate, which is a necessary step in validation of wind-tunnel integrity with the test models, an experimental model was constructed using an instrumented smooth flat plate. The model was in essence a large composite of many heat-flux gauges and guard heaters, a sectional view of which is shown in Fig. 1. The test bed consisted of a center row of test tiles, each being approximately 0.017 m in the flow direction, 0.029 m perpendicular to the flow direction, and 0.013 m deep. Biot number calculations[16] showed that such dimensions were suitable for the assumption of a constant locally averaged temperature for each tile. Four guard tiles, each being approximately 0.117 m in the flow direction, 0.032 m perpendicular to the flow direction, and 0.013 m deep, were placed along each side of the center tiles. To provide heat, each center tile was instrumented with a standard thermofoil heater, which was 0.013 × 0.025 m (31.6 ohms), and each side guard tile was instrumented with a 0.025 × 0.076 m (52.3 ohms) heater.

On one side of each of the center test tiles and each of the eight side strips, a 0.002-m diam, 0.006-m deep hole was drilled 0.006 m from the bottom of each tile. Each hole housed the bead of a thin Chromel-Alumel thermocouple to measure the average temperature of the tile, as shown in Fig. 1.

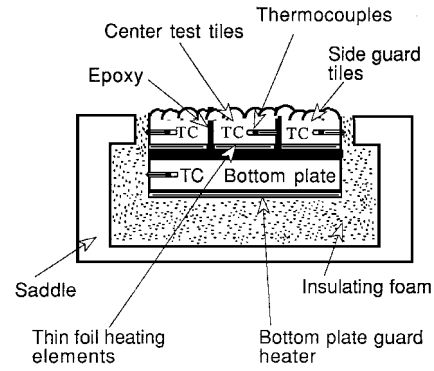

Fig. 1 Sectional view of the heat-transfer model.

The center test tiles and the side guard tiles were all glued together using epoxy and plastic spacing shims to ensure a uniform gap between all of the tiles and to thermally insulate the tiles from each other. This top part was then glued to a large bottom plate fabricated from 0.013-m thick aluminum plate. A standard 35.9 ohms, 0.076 × 0.381 m thermofoil heater was affixed to the bottom surface of this plate. This plate served as the bottom guard heater to prevent conduction downward and provided the primary structural support for the model. The whole structure was then placed in a milling machine, and its top surface was machined smooth (surface roughness, after machining, averaged 3.2×10^{-10} m).

To construct the roughness models, a characteristic roughness of the natural ice shapes was chosen from one of the cast 356-aluminum plates. Twenty-two center test tiles and eight side tiles were cut using an Electrical Discharge Machine (EDM) to minimize the metal loss from cutting and thus preserving the actual roughness elements' integrity. To maintain surface flow symmetry, the 22 tiles and eight side strips had the same roughness pattern and shape representing the desired roughness characteristic for the model under construction. The process of construction was identical to that of the smooth model (with the surface roughness intact) and was repeated to complete a total of seven different roughness models. The construction of model 2 was slightly different from the others in that it was intentionally fabricated so that the roughness density was not uniform but decreased gradually starting at the 10th tile from the leading edge. The purpose of this design was to determine if the heat transfer would be completely governed by the roughness character of the initial region. The average spacing of 15.09×10^{-3} m in Table 2 for model 2 therefore has a wider span in its value than do the average spacings of the other six models. Figure 2 shows a sample of the roughness pattern of each of the seven models.

Characterization of Roughness

Three independent roughness quantities were obtained for roughness models 1–7 and are shown in Table 2. The average roughness height $\bar{H}$ and the average spacing $\bar{S}$ were measured using a machinist indicator with a needle point and a dial accurate to 2.5×10^{-5} m (0.001 in.). Precise measurements of the surface area were obtained by Cyberware, Inc., Monterey, CA, using a CYBERWARE MODEL 3030 three-dimensional laser digitizer. The high sensitivity of the digitizer accommodated the surface properties of the roughness models. The scanning process captured an array of digitized points, with each point represented by xyz coordinates in μm. The measurement grid along each roughness model was 2.5×10^{-4} m, 3.5×10^{-4} m across, and 1.0×10^{-4} m perpendicular to the surface. These measurements produced a statistically significant sample from which the surface area for each roughness model A_{rgh} was computed.

Both the surface area increase because of roughness and the roughness element height cause higher heat-transfer rates than from a smooth surface. An increase in the roughness element spacing, in general, reduces this increase in the heat-transfer rate. Based on

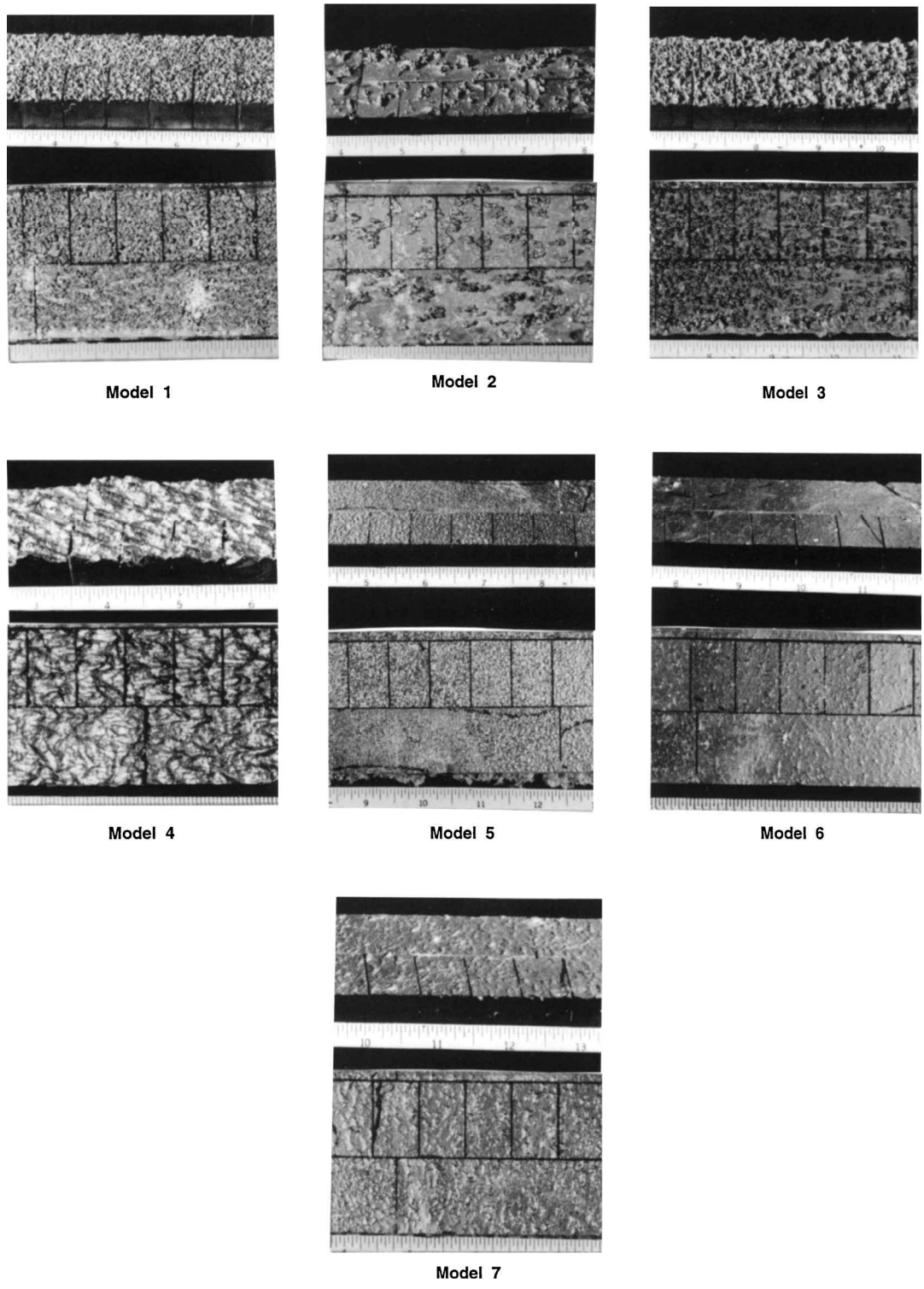

Fig. 2 Perspective and top view of roughness patterns.

these observations, and in order to characterize the roughness patterns of each of the models used in this study, the following dimensionless combination was formed and was termed Index of Random Roughness (IRR):

$$\text{IRR} = \left(\frac{A_{\text{rgh}}}{A_{\text{smth}}}\right) \times \left(\frac{\bar{H}}{S}\right) \tag{1}$$

This combination reduces to zero for a smooth surface ($\bar{H} \rightarrow 0$, $S \rightarrow \infty$). Values of IRR for the roughness models 1–7 are shown in Table 2.

Wind-Tunnel Testing and Data Reduction

Experiments were carried out in the wind tunnel shown schematically in Fig. 3 and described in detail by Van Fossen et al.[17] The John H. Glenn Research Center's ESCORT data acquisition system was utilized. A removable and adjustable structure, called the saddle (Fig. 3), was used to mount the models in the wind-tunnel test section. This permitted accurate model placement and alignment, and also ensured a smooth uniform airflow onto the heat-transfer model without any separation bubbles. The front part of the saddle constituted an unheated starting length of approximately 0.052 m. Heat-transfer data for the smooth flat plate and for each of the seven models were collected for the freestream velocities of 9.4, 20.7,

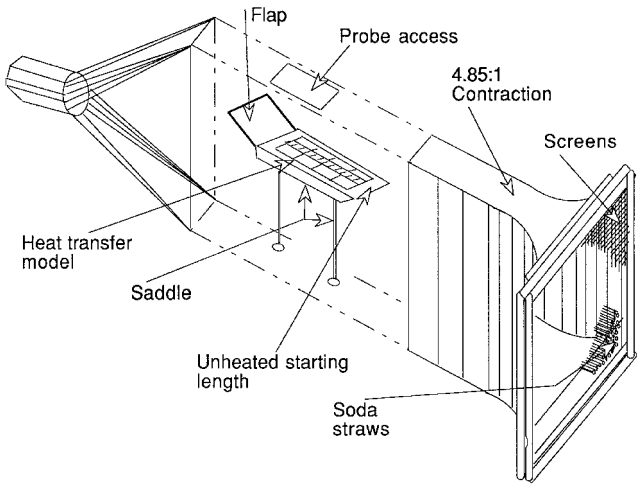

Fig. 3 Schematic of wind tunnel with heat-transfer model installed.

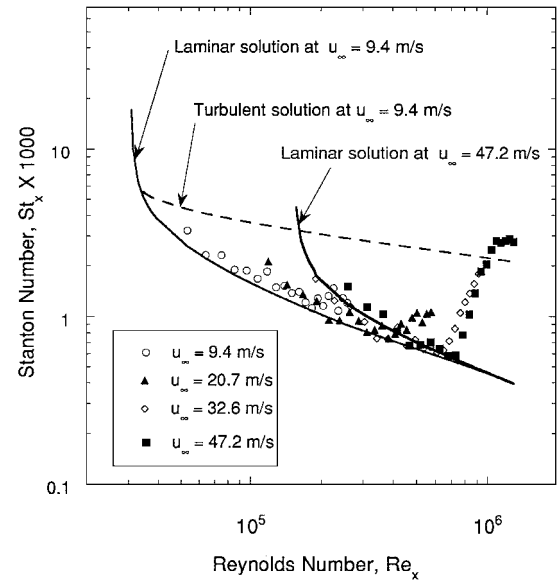

Fig. 4 Stanton number vs Reynolds number: smooth model results.

32.6, and 47.2 m/s and with a surface-to-freestream temperature difference of approximately 20.5°C.

The desired flow rates in the tunnel were established and were allowed to reach steady state before data were taken. The freestream turbulence level was under 0.5% throughout the experiment. A control circuit automatically adjusted the power input to each tile so that all tiles were within ±0.25°C of the set value. To eliminate conductive losses, the guard tiles and the bottom plate were maintained at the same temperature. The power input to each tile (energy flux), which compensated for the heat loss by convection from the top surface, was recorded and, along with the surface and tunnel temperatures, provided the needed information for the heat-transfer coefficient calculations.

Reduction of the raw data was performed by a computer code that was developed, used, and then was modified by Van Fossen et al.[17] The locally averaged Stanton number $St_x = h/\rho c_p u_\infty$ for each gauge was determined by subtracting the heat losses from the measured power input to each of the individual tiles. The radiation loss was on the order of 0.2%, and it was calculated assuming gray body radiation to black surroundings and an emissivity of 0.05 for the aluminum tiles. The loss caused by the epoxy gap between the test tiles was about 2%, and it was obtained from an exact solution for two-dimensional conduction in a rectangular slab.[17] At high heat fluxes a significant temperature gradient developed between the heater and the imbedded thermocouple. This gradient made it impossible to adjust the bottom guard temperature to exactly match the heater temperature, thus allowing a small amount of heat to leak to the bottom of the guard, which was accounted for by assuming one-dimensional heat conduction. The gap loss was also about 2% of the total heat flow.

The measurement uncertainty associated with the results of this study, using the method of Kline and McClintock,[18] averaged 5.7% and reached a maximum of 7.8%.

Results

Smooth Model Results

Figure 4 shows the Stanton number vs the Reynolds number for the smooth flat plate model at the four freestream velocities. The experimental values are compared to the theoretical values obtained from the well-accepted solution for laminar flow over a smooth surface with an unheated starting length[19]:

$$St_x = \frac{0.332\, Re_x^{-\frac{1}{2}} Pr^{-\frac{2}{3}}}{\left[1 - (x_o/x)^{\frac{3}{4}}\right]^{\frac{1}{3}}} \tag{2}$$

The experimental data are shown to conform to the preceding solution, within experimental error, up to transition. Equation (2) is shown for the freestream velocities of 9.4 and 47.2 m/s by the solid lines on Fig. 4. Note that transition occurs for the freestream velocity of 9.4 m/s at a local Reynolds number of approximately 2×10^5, where there is a rise in the Stanton number. Corresponding transition Reynolds numbers for freestream velocities of 20.7, 32.6, and 47.2 m/s are 4×10^5, 6×10^5, and 7×10^5, respectively. In the heat-transfer sense the onset of transition was defined by Keller,[20] among others, as the point of minimum Stanton number at which it deviates from the corresponding laminar case and starts rising, and the end of transition as the point of maximum Stanton number immediately following the rise. Also plotted on Fig. 4 is the well-known solution for turbulent flow over a smooth surface with an unheated starting length[19,20] given by

$$St_x = 0.03\, Pr^{-0.4} Re_x^{-0.2}\left[1 - (x_o/x)^{0.9}\right]^{-\frac{1}{9}} \tag{3}$$

Roughness Models Results

In roughness studies[1,2,6,8,21] the flow regimes are usually classified as aerodynamically smooth and fully rough. The flow regime in between these two is termed transitional or transitionally rough. In the smooth regime the roughness element height is less than that of the viscous sublayer; hence, the outer flow does not sense the roughness elements, and viscous effects dominate. In this regime the skin-friction coefficient is the same function of the gross flow Reynolds number as for a smooth surface without the roughness elements. In the transitionally rough regime the roughness elements begin to protrude through the sublayer, and both the viscous and roughness effects are important. In this regime the skin-friction coefficient is a function of both the flow Reynolds number and the roughness character of the surface. Finally, in the fully rough regime the roughness height is greater than the viscous sublayer height. Therefore, the sublayer is said to be fully destroyed, and the viscous effects become insignificant. The flow is then controlled by the roughness effects alone, and the skin-friction coefficient is independent of the flow Reynolds number.

In most roughness studies the flow regime classification relied on the definition and value of certain fluid parameters. Nikuradse[1] defined a range of values of a roughness Reynolds number, containing both the friction velocity and the size of the sandgrain roughness as a length scale, in order to classify his flow regimes. Pimenta[21] proposed the use of the Reynolds stress tensor component $(u')^2$ profiles for roughness flow regime classification. Coleman et al.[22] suggested using the ratio of the apparent shear stress due to the roughness elements to the total apparent shear stress as calculated using the discrete element method, R_τ, to classify the roughness flow regimes.

Some roughness studies attempted to use certain heat transfer parameters to classify the flow regimes. Pimenta,[21] for example, stated that in the fully rough regime, the Stanton number was independent of the Reynolds number. Healzer et al.[23] observed the same behavior at higher freestream velocities. Pimenta also used the independence of the Stanton number, when plotted vs the enthalpy thickness divided by the radius of a spherical roughness element, from the freestream velocity as an indication of the fully rough flow regime. However, Hosni et al.[6] showed that, for their data, Pimenta's classifications of the flow regimes based on the Reynolds number independence were not consistent with the Reynolds stress criteria $(u')^2$ or with the R_τ criteria.[22] Hosni et al.[6] suggested using the ratio of the rate of heat transfer from the roughness elements to the fluid to the total rate of heat transfer from the surface to the fluid as a parameter for classification. A major conclusion presented by Hosni et al.[6] was that roughness flow regime classifications could not be made based on Stanton number vs local Reynolds number data alone, nor could they be determined from the Stanton number asymptotic behavior when plotted vs enthalpy thickness. Hosni et al.[6] achieved success using the discrete element method model predictions for flow classifications when compared with the fluid dynamic criteria. In a later study Hosni et al.[8] observed differences in Stanton-number measurements depending on roughness element shape, whereas no differences were evident in the friction coefficient data.

In the present study no detailed fluid mechanical measurements of the flowfield, such as hot wire data, were taken, nor were any numerical codes used for predictions. The classifications of the flow regimes used in the data interpretation of this study are restricted to the traditional laminar and turbulent flow definitions and do not include the roughness flow regimes already mentioned.

For discussion purposes the roughness models considered in this investigation can be grouped into four ice roughness categories, as stated in Tables 1 and 2: rime feathers (model 4), rough glaze (models 1–3), smooth rime (models 5 and 7), and smooth glaze (model 6).

Two composite plots of Stanton number vs the local Reynolds number for the freestream velocities of 9.4 and 47.2 m/s are shown in Figs. 5 and 6, respectively. In Fig. 5 for a freestream velocity of 9.4 m/s models 1–3 (all rough glaze) show comparable Stanton numbers up to $Re_x = 10^5$, whereas model 4 (rime feathers) has

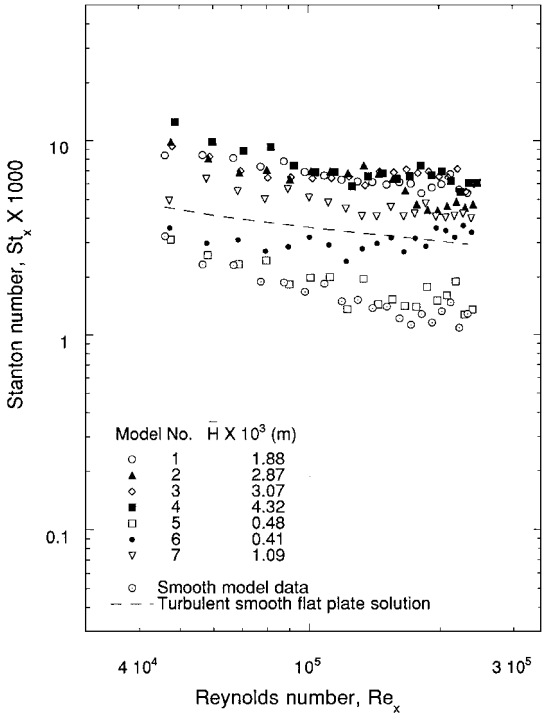

Fig. 5 Stanton number vs Reynolds number: comparison of the roughness models at u_∞ = 9.4 m/s.

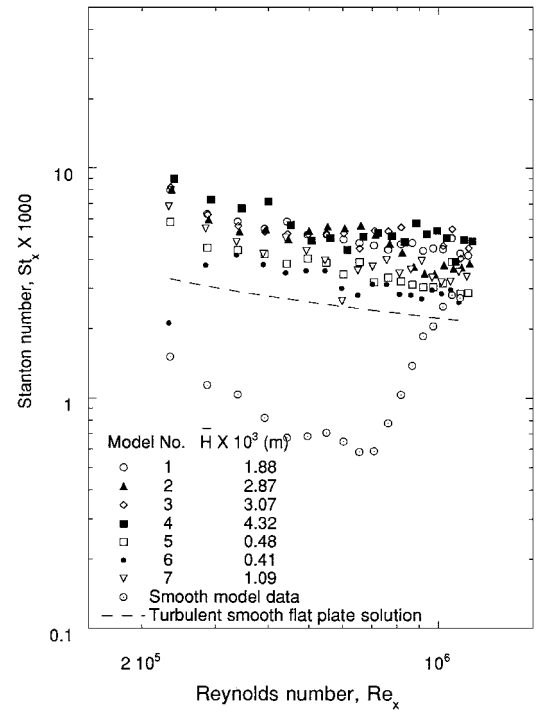

Fig. 6 Stanton number vs Reynolds number: comparison of the roughness models at u_∞ = 47.2 m/s.

somewhat higher values. The Stanton number values for these four models are essentially equal at $Re_x = 10^5$, after which an almost constant asymptotic behavior between $St_x = 0.006$ and 0.007 is observed for higher Re_x for models 1, 3, and 4. Model 2, the last 10 tiles of which have larger roughness spacing as discussed in the Model Construction section, shows, as a consequence, a severe drop in Stanton number at approximately $Re_x = 1.5 \times 10^5$. For greater Re_x model 2 shows values of St_x between 0.004 and 0.005. For roughness model 7 (smooth rime) the Stanton numbers are lower than those for models 1–4. Transition to turbulence for this model is observed over the first few tiles from the leading edge. An almost constant asymptotic St_x of about 0.004 is reached after a Re_x of approximately 2×10^5. Correspondingly, model 5, closely spaced smooth rime, has much lower Stanton number values and behaves as the smooth model for this freestream velocity, with transition being indicated at $Re_x = 2 \times 10^5$. From Table 2, even though the roughness spacing for model 5 is more dense (which tends to increase the rate of heat transfer) as vs model 7, the roughness height for model 5 is less, and this appears to be the controlling factor in the rate of heat transfer. Finally, model 6 (smooth glaze) has its transition onset at about $Re_x = 6 \times 10^4$, with almost complete transition at $Re_x = 2 \times 10^5$. On a macroscopic scale models 5 and 7 and models 6 and 7 show a dependence of higher Stanton number corresponding to higher roughness element height, although models 5 and 6 do not. Model 4 only indicates this dependence up to $Re_x = 10^5$, whereas the data for models 1–3 are almost indistinguishable over the range of local Reynolds numbers and do not show this dependence on $\bar{H}$.

Some similarities to the behavior in Fig. 5 are noted in Fig. 6 for a freestream velocity of 47.2 m/s. Again models 1–3 have comparable St_x values, with model 4 being higher, except that the local Reynolds number at which the data merge is 5×10^5 as vs 10^5 for the lower freestream velocity. The Stanton number behavior for models 1, 3, and 4 for Re_x greater than 5×10^5 is between approximately $St_x = 0.004$ and 0.005, although scatter in the data is present. Roughness model 2 exhibits the same behavior as in Fig. 5, with a severe drop in the data at $Re_x = 7 \times 10^5$ and final Stanton number values between 0.0035 and 0.004. The Stanton-number curve for roughness model 7 now reflects turbulent flow for the whole range of Re_x. It declines starting at the leading edge up to $Re_x = 4 \times 10^5$ and, with some scatter, has St_x values between 0.003 and 0.004 for Re_x greater than 5.5×10^5. Roughness model 5, at this higher

freestream velocity, now also shows fully turbulent behavior over the whole range of Re_x. Roughness model 6 has its onset of transition at the first tile. The transition is completed at about $Re_x = 3.5 \times 10^5$. For this higher freestream velocity one can see that there is a large increase in magnitude of the Stanton numbers for both models 5 (smooth rime) and 6 (smooth glaze). Because these models had the smallest roughness element heights $\bar{H}$, the increase in freestream velocity was needed in order for the roughness elements to be felt and have a significant effect on both the flow regime and on the surface heat transfer. In this different flow regime an inversion of St_x magnitude occurs between Figs. 5 and 6 for these two models. As was observed in Fig. 5, no dependence on $\bar{H}$ is seen in Fig. 6 for models 1–3, and model 4 indicates this dependence only for Re_x up to 10^5. Models 5–7, in this turbulent flow regime, now tend to show this dependence, with some scatter, over the whole range of local Reynolds numbers.

In general, from the data in Figs. 5 and 6, the rime feather ice roughness (model 4) produced the highest heat-transfer rate followed by the rough glaze roughness (models 1–3). The smooth rime (models 5 and 7) and the smooth glaze roughness (model 6) produced lower rates of heat transfer, respectively, and show a heat-transfer dependence proportional to the roughness element heights in the turbulent flow regime. Similar trends were observed for the intermediate velocities of 20.7 and 32.6 m/s (Ref. 16).

Figures 7 and 8 provide an assessment of the effect of the freestream velocity on the Stanton number for two different types of ice roughness. Figure 7 shows the typical behavior of the Stanton number of the rough glaze family represented by roughness model 1 at different freestream velocities, and Fig. 8 shows the same information for the smooth rime ice family represented by roughness model 5. In Fig. 7 the Stanton numbers for all four freestream velocities are in the fully turbulent state. The family of curves that are initially distinct, and start at higher values for higher freestream velocities, is caused by the presence of the unheated starting length. The curves are shown to collapse onto a single curve and become a function of the Reynolds number only at approximately $Re_x = 3.2 \times 10^5$. Similar observations were made in the roughness studies of Hosni et al.[6,8] and Pimenta.[21]

Figure 8 shows the Stanton numbers for roughness model 5. This model behaves as a smooth surface for the low freestream velocity of 9.4 m/s. The onset of transition of this model at this velocity is at approximately $Re_x = 2 \times 10^5$. For $u_\infty = 20.7$ m/s the onset of

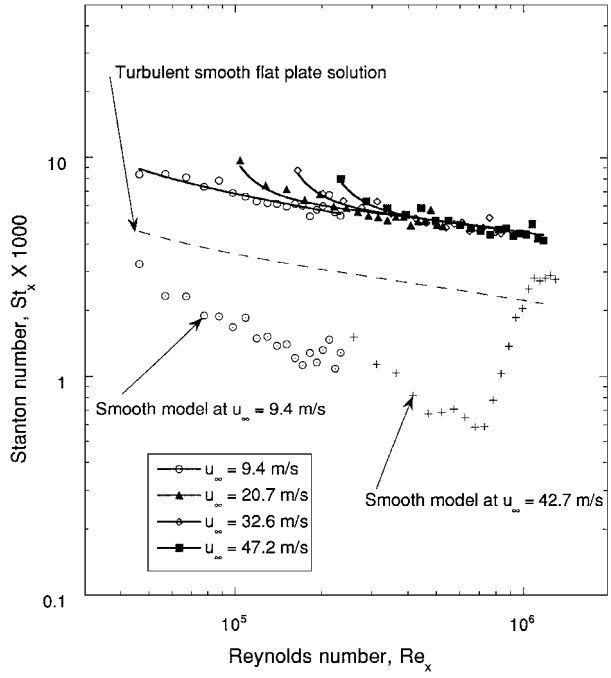

Fig. 7 Stanton number vs Reynolds number: roughness model 1 at different freestream velocities.

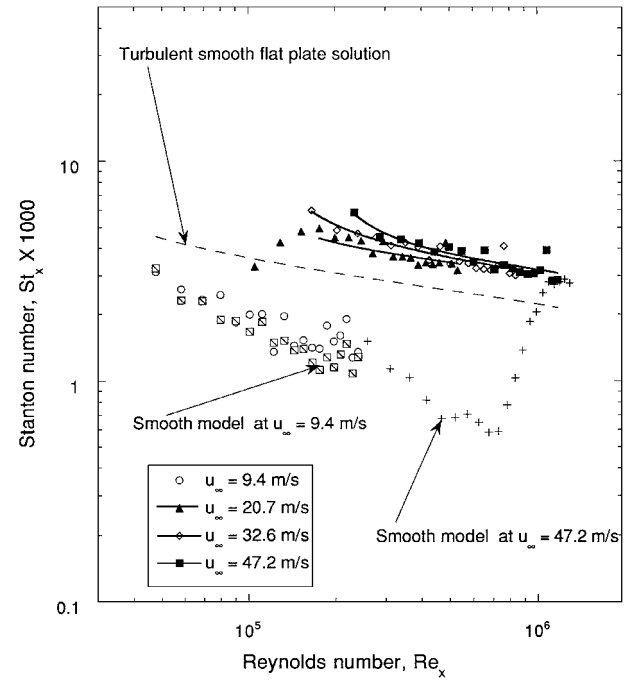

Fig. 8 Stanton number vs Reynolds number: roughness model 5 at different freestream velocities.

transition is at about $Re_x = 10^5$, and transition is completed at about $Re_x = 2 \times 10^5$. The Stanton-number data for the higher freestream velocities of 32.6 and 47.2 m/s are in the fully turbulent state. The curves for the three higher freestream velocities collapse onto a single curve at approximately $Re_x = 3 \times 10^5$.

Comparisons to Organized Roughness

Comparisons were made with two previous studies in order to contrast the heat transfer in the random roughness element case (ice roughness) with that for two well-defined roughness elements cases, i.e., hemispheres and truncated cones. To avoid repetition of similar data, roughness models 1, 4, 5, and 7 were chosen for the comparisons.

Hosni et al.[6] studied the heat-transfer behavior for hemispherical roughness elements spaced 2, 4, and 10 diameters apart on otherwise smooth surfaces. The freestream velocity of 42.7 m/s in Hosni et al.'s study was chosen for comparison with the case for the freestream velocity of 47.2 m/s of this study. This was decided for two reasons: 1) the relatively small difference between the two values of the freestream velocity and 2) the fact that for these velocities the heat transfer was in the fully developed turbulent state for both studies. In the fully turbulent state no transitional effects are present, and the Stanton-number curves approach an asymptotic behavior, which allows for easier comparisons. Hosni et al. were also able to classify their flow regimes as transitionally rough ($L/d = 10$) and fully rough ($L/d = 2, 4$). These classifications could not be used in the present study because no detailed flow measurements were taken and no predictive codes were used. As shown in Fig. 9, Hosni et al.'s[6] Stanton-number data for the surface with the highest roughness density, $L/d = 2$, are of approximately the same magnitude as the data for two of the least rough surfaces of this study. These are the cases for models 5 and 7, which are castings of smooth rime ice. The data for the rough glaze ice (model 1) and the rime ice feather roughness (model 4) show significantly higher rates of heat transfer. Hosni et al.'s[6] data for their other two rough surfaces, $L/d = 4$ and 10, lie below the previous data, which is believed to be caused by larger roughness element spacing. The Stanton-number behavior for the random roughness models of the current study indicates a dependence on element height $\bar{H}$ for the ranges of $Re_x < 4.5 \times 10^5$ and $Re_x > 8.5 \times 10^5$, although between these regions there is considerable overlap of the data.

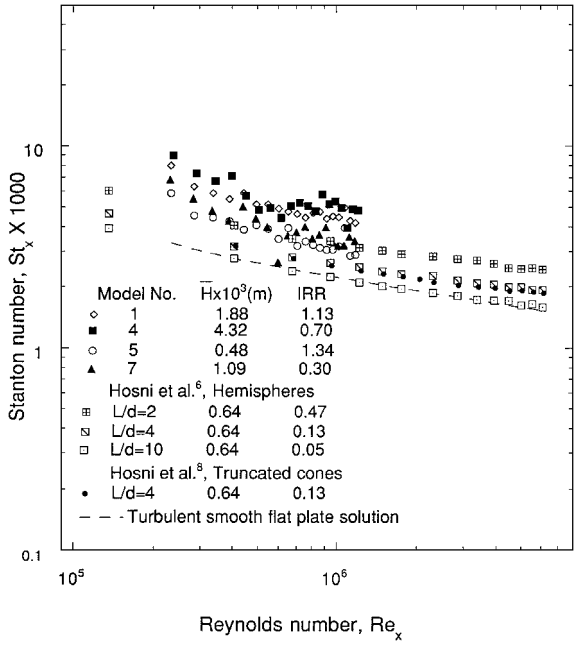

Fig. 9 Stanton number vs Reynolds number: comparison with Hosni et al.[6] and Hosni et al.[8] at $u_\infty = 47.2$ m/s.

Figure 9 also shows a comparison with Hosni et al.[8] for truncated cones spaced 4 base diameters apart at a freestream velocity of 43.1 m/s. Hosni et al.[8] also reported data for cones being spaced 2 base diameters apart. The Stanton-number data for the $L/d = 4$ case are again lower than those for the roughness models of this study. As Hosni et al.[8] observed, their data, for the same roughness element height, correlate well with L/d, but do show a dependence on roughness element shape (between hemispheres and truncated cones), which they believe to be real and physically meaningful. Hosni et al.'s data also correlate with the IRR used in the present study. However, the IRR for the common $L/d = 4$ case has the same value of 0.13 for the hemisphere and truncated cone elements and therefore does not show, as presently defined, a shape sensitivity for these two different well-defined roughness elements.

Although there are differences between the roughness heights and spacings between the current study and those by Hosni et al.,[6,8] there is also some overlap. It therefore appears that the increased rate of heat transfer in the case of ice roughness as vs the hemispherical and truncated cone roughness may be attributed to the difference in roughness element shape. The percentage increase in the Stanton number for the seven models used in this study over that for the smooth model is given in the last column of Table 2.

Correlations

Correlations of Stanton Number

Most of the available forced convection heat-transfer correlations for both laminar and turbulent flows over surfaces with unheated starting lengths are expressed in terms of power laws of the form

$$St_x = a\, Re_x^m\, Pr^n \left[1 - (x_o/x)^\phi\right]^\eta \tag{4}$$

For fully turbulent flow over a smooth surface, the constant a is usually 0.03, m is -0.2, and n is -0.4. The exponents ϕ and η vary from one empirical correlation to another; ϕ is usually 0.9 or 1.0, and η is $-\frac{1}{9}$, as discussed by Kays,[19] Keller,[20] and Madavan and Rai.[24]

With $Pr = 0.707$ and $n = -0.4$, Eq. (4) was used to fit the experimental data of this investigation employing the least-square-fit method (see Ref. 16). Values of the constants a, m, ϕ, and η for each roughness model at each freestream velocity, after transition, were obtained and are shown in Table 3. The power fits are shown by the solid lines in Figs. 7 and 8. The correlation coefficient was greater than 0.9 for most of the cases considered, and 91% of the data were predicted by the correlation to within ±10%.

Table 3 Correlation constants

Model no.	u_∞, m/s	a	m	ϕ	η
1	9.4	0.036	−0.180	0.104	−0.126
	20.7	0.038	−0.163	4.685	−2.323
	32.6	0.038	−0.163	4.860	−2.495
	47.2	0.038	−0.164	4.922	−2.385
2	9.4	0.029	−0.214	0.019	−0.223
	20.7	0.034	−0.197	0.092	−0.242
	32.6	0.033	−0.196	0.099	−0.258
	47.2	0.034	−0.198	0.086	−0.247
3	9.4	0.024	−0.119	7.529	−6.931
	20.7	0.032	−0.147	10.46	−34.460
	32.6	0.034	−0.152	10.70	−32.329
	47.2	0.035	−0.155	9.282	−18.960
4	9.4	0.034	−0.151	2.004	−1.048
	20.7	0.035	−0.150	5.282	−4.948
	32.6	0.035	−0.151	3.832	−2.333
	47.2	0.034	−0.153	2.223	−0.951
5	9.4	——	——	——	——
	20.7	0.034	−0.185	3.072	−1.210
	32.6	0.036	−0.190	1.371	−0.415
	47.2	0.037	−0.188	2.226	−0.670
6	9.4	——	——	——	——
	20.7	0.031	−0.190	0.099	−0.036
	32.6	0.033	−0.188	3.127	−2.402
	47.2	0.033	−0.189	2.517	−1.482
7	9.4	0.034	−0.189	0.049	−0.026
	20.7	0.034	−0.177	3.858	−2.016
	32.6	0.035	−0.176	4.291	−2.474
	47.2	0.034	−0.178	2.221	−0.903

Correlations of the Constants a and m

For a fixed Prandtl number and in the fully turbulent regime and where the effect of the unheated starting length is not present, the Stanton number is a function of the Reynolds number only, and the constants a and m are sufficient to determine the asymptotic values of the Stanton number $St_x = a\, Re_x^m\, Pr^{-0.4}$.

An exponential curve fit that would reduce to the well-known value of a for the turbulent flow over a smooth plate ($\bar{H} = 0$), 0.03 was used to fit the values of the constant a. The variation of a as a function of IRR is given by

$$a = 0.040 - 0.010 \exp\left(-\sqrt{\text{IRR}}\right) \tag{5}$$

The constant m was directly related to the average roughness height $\bar{H}$ only. An exponential curve fit for m as a function of $\bar{H}$ is given by

$$m = -0.049 - 0.153 \exp\left(-\sqrt{\bar{H}}\right) \tag{6}$$

which also reduces to the smooth surface value of m, i.e., -0.2.

Conclusions

Stanton-number results were obtained for the rate of convective heat transfer from aluminum castings of ice-roughened surfaces. The castings were obtained from stochastically accreted ice on flat surfaces in the IRT at the John H. Glenn Research Center. Four basic types of ice accretions were considered: smooth glaze, smooth rime, rough glaze, and rime ice feathers. Seven models representing the four different types of ice accretions were tested in a wind tunnel for freestream velocities of 9.4, 20.7, 32.6, and 47.2 m/s. For the lower freestream velocity of 9.4 m/s, the closely spaced smooth rime model behaved as a smooth surface in laminar flow, and the smooth glaze model was in the laminar-turbulent transitional state. For these two models the roughness element heights were too small to significantly affect the heat transfer. The other five of the models were in the fully turbulent regime, and the Stanton numbers for certain models increased with increasing roughness element height; but this was not true for all of the models over the complete range of local Reynolds numbers. For the higher freestream velocity of 47.2 m/s, only the smooth glaze model (lowest roughness height)

was in the transitional regime, with the other models being in the fully turbulent regime. Again, some dependence of Stanton-number magnitude on the roughness element height was noticed, but it was not universal for all models for the whole range of local Reynolds numbers. In general, the highest rate of heat transfer was produced by the rime ice feathers roughness (model 4) followed by the rough glaze roughness (models 1–3), smooth rime roughness (models 5 and 7), and the smooth glaze roughness (model 6). The Stanton numbers obtained in this study were higher than those obtained in heat-transfer roughness studies using hemispherical and truncated cone roughness elements, which indicates that roughness element shape is a primary factor affecting the rates of heat transfer. The complete data set for the Stanton number was correlated as a function of the local Reynolds number using a newly defined IRR parameter and the roughness element height to characterize the accreted ice shapes. The data obtained can be used to effectively size and design in-flight deicing systems and can also be used in numerical codes for predictions of accreted ice shapes.

Acknowledgments

The authors express their gratitude to the Icing and Cryogenics Technology Branch at the John H. Glenn Research Center at Lewis Field for funding this effort under Grant NAG 3-72 and the Heat Transfer Branch for their help and allowing the use of their facilities, especially Jaiwon Shin, Mario Vargas, and David Anderson.

References

[1]Nikuradse, J., "Laws of Flow in Rough Pipes," NACA TM 1292, Nov. 1950.

[2]Schlichting, H., "Experimental Investigation of the Problem of Surface Roughness," NACA TM 823, April 1937.

[3]Simpson, R. L., "Generalized Correlation of Roughness Density Effects on the Turbulent Boundary Layer," *AIAA Journal*, Vol. 11, No. 2, 1973, pp. 242–244.

[4]Dirling, R. B., Jr., "A Method for Computing Rough Wall Heat Transfer Rates on Reentry Nosetips," AIAA Paper 73-763, July 1973.

[5]Coleman, H. W., Hodge, B. K., and Taylor, R. P., "A Re-Evaluation of Schlichting's Surface Roughness Experiment," *Journal of Fluids Engineering*, Vol. 106, No. 1, 1984, pp. 60–65.

[6]Hosni, M. H., Coleman, H. W., and Taylor, R. P., "Measurement and Calculations of Rough Wall Heat Transfer in the Turbulent Boundary Layer," *International Journal of Heat and Mass Transfer*, Vol. 34, No. 4, 1991, pp. 1067–1082.

[7]Lewis, M. J., "An Elementary Analysis for Predicting the Momentum- and Heat-Transfer Characteristics of Hydraulically Rough Surface," *Journal of Heat Transfer*, Vol. 97, No. 2, May 1975, pp. 249–254.

[8]Hosni, M. H., Coleman, H. W., and Garner, J. W., "Roughness Shape Effect on Heat Transfer and Skin Friction in Rough-Wall Turbulent Boundary Layer," *International Journal of Heat and Mass Transfer*, Vol. 36, No. 1, 1993, pp. 147–153.

[9]Coleman, H. W., "Momentum and Energy Transport in the Accelerated Fully Rough Turbulent Boundary Layer," Ph.D. Dissertation, Dept. of Mechanical Engineering, Stanford Univ., Stanford, CA, March 1976.

[10]Hosni, M. H., Coleman, H. W., and Taylor, R. P., "Calculations of Rough-Wall Heat Transfer in the Turbulent Boundary Layer," AIAA Paper 91-0161, Jan. 1991.

[11]Poinsatte, P. E., "Heat Transfer Measurements from a NASA 0012 Airfoil," *Journal of Aircraft*, Vol. 28, No. 12, 1991, pp. 892–898.

[12]Poinsatte, P. E., "Roughness Effect on Heat Transfer from a NASA 0012 Airfoil," *Journal of Aircraft*, Vol. 28, No. 12, 1991, pp. 908–911.

[13]Pais, M., Singh, S., and Zou, L., "Determination of the Local Heat Transfer Characteristics on Simulated Smooth Glaze Ice Accretions on a NASA 0012 Airfoil," AIAA Paper 88-0292, Jan. 1988.

[14]Wright, W. B., "User Manual for the Improved NASA Lewis Ice Accretion Prediction Code LEWICE 1.6," NASA CR 198355, June 1995.

[15]Wood, R. L., and Von Ludwig, D., *Investment Casting for Engineers*, Reinhold, New York, 1952, pp. 5–15.

[16]Dukhan, N., "Measurements of the Convective Heat Transfer Coefficient from Ice Roughened Surfaces in Parallel and Accelerated Flows," Ph.D. Dissertation, Dept. of Mechanical, Industrial and Manufacturing Engineering, The Univ. of Toledo, Toledo, OH, Dec. 1996.

[17]Van Fossen, G. J., Simoneau, R. J., Olsen, W. A., Jr., and Shaw, R. J., "Heat Transfer Distributions Around Nominal Ice Accretion Shapes Formed on a Cylinder in the NASA Lewis Icing Research Tunnel," AIAA Paper 84-0017, Jan. 1984.

[18]Kline, S. J., and McClintock, F. J., "Describing Uncertainties Analysis in Single Sample Experiment," *Mechanical Engineering Journal*, Vol. 75, No. 1, 1953, pp. 3–8.

[19]Kays, W. M., *Convective Heat and Mass Transfer*, McGraw–Hill, New York, 1966, pp. 214–217.

[20]Keller, F. J., "Flow and Thermal Structure in Heated Transitional Boundary Layers With and Without Stream-Wise Acceleration," Ph.D. Dissertation, Dept. of Mechanical Engineering, Clemson Univ., Clemson, SC, Aug. 1993.

[21]Pimenta, M. D., "The Turbulent Boundary Layer: An Experimental Study of the Transport of Momentum and Heat Transfer with the Effect of Roughness," Ph.D. Dissertation, Dept. of Mechanical Engineering, Stanford Univ., Stanford, CA, May 1975.

[22]Coleman, H. W., Hodge, B. K., and Taylor, R. P., "Generalized Roughness Effects on Turbulent Boundary Layer Heat Transfer—A Discrete Element Predictive Approach for Turbulent Flow over Rough Surfaces," Air Force Armament Lab., AFTL-TR-83-90, Eglin AFB, FL, Nov. 1983.

[23]Healzer, J. M., Moffat, R. J., and Kays, W. M., "The Turbulent Boundary Layer on a Porous, Rough Plate: Experimental Heat Transfer with Uniform Blowing," AIAA Paper 74-680, July 1974.

[24]Madavan, N. K., and Rai, M. M., "Direct Numerical Simulation of Boundary Layer Transition on a Heated Flat Plate with Elevated Free-Stream Turbulence," AIAA Paper 95-0771, Jan. 1995.